RESEARCH ARTICLE

An NIR triphenylamine grafted BODIPY derivative with high photothermal conversion efficiency and singlet oxygen generation for imaging guided phototherapy†

Jianwei Zhu,‡[ab] Jianhua Zou,‡[b] Zhanjie Zhang,[a] Jie Zhang,[a] Yang Sun,[a] Xiaochen Dong*[b] and Qi Zhang [ID] *[a]

Osteosarcoma, the most common malignant bone tissue tumor, with a high degree of malignancy, strong metastasis, and early lung metastasis, can result in extremely high mortality, and is a serious threat to human health. Boron dipyrromethene (BODIPY) compounds have shown great potential in photodynamic tumor therapy. In this study, an NIR triphenylamine grafted BODIPY derivative (BDPTPA) with high singlet oxygen generation efficiency (35.2%) was designed and synthesized. BDPTPA nano-particles (NPs) obtained by nanoprecipitation present high photothermal conversion efficiency (52.6%). Both MTT assay and flow cytometry experiments suggest that BDPTPA NPs are able to generate high photo-toxicity and induce apoptosis of osteosarcoma cells, while presenting negligible dark-toxicity towards osteosarcoma cells as well as normal human cells. Cell migration and transwell experiments demonstrate that BDPTPA NPs can inhibit the migration of osteosarcoma cells. Due to the enhanced permeability and retention (EPR) effects, BDPTPA NPs can accumulate in tumor tissue in 6 h. Pharmacokinetic studies in rats indicate that BDPTPA NPs eliminate much more slowly than BDPTPA in 10% DMSO. Under the irradiation of an 808 nm laser, in *in vivo* experiments, BDPTPA NPs can significantly inhibit tumor growth without side effects towards normal tissues. BDPTPA NPs show good biosafety and excellent therapeutic effect both *in vitro* and *in vivo*, indicating their great potential for treatment of osteosarcoma.

Introduction

Osteosarcoma, including primary bone tumors and metastatic bone tumors,[1] accounts for about 1% of all malignant tumors.[2] Osteosarcoma is the most common tumor that occurs in children and young adults, and has a high rate of death and disability, and its current five-year survival rate is about 65–75%.[3–7] The diagnosis and treatment of osteosarcoma is still a difficult problem because the location of the tumor is deep in the bone tissue.[8]

At present, surgery and chemotherapy play significant and crucial roles in clinical osteosarcoma treatment.[9] Although the

[a] *School of Pharmaceutical Sciences, Nanjing Tech University (NanjingTech), 30 South Puzhu Road, Nanjing 211816, China. E-mail: zhangqi@njtech.edu.cn*

[b] *Key Laboratory of Flexible Electronics (KLOFE) & Institute of Advanced Materials (IAM), Jiangsu National Synergetic Innovation Centre for Advanced Materials (SICAM), Nanjing Tech University (NanjingTech), 30 South Puzhu Road, Nanjing 211816, China. E-mail: iamxcdong@njtech.edu.cn*

† Electronic supplementary information (ESI) available. See DOI: 10.1039/c9qm00044e

‡ These authors contribute equally to this work.

principle of surgery is to remove the tumor as completely as possible, osteosarcoma often has invasive growth, close adhesion to surrounding tissues, and strong recurrence, leading to difficulty in removing the tumor tissue completely.[10] Surgery usually combines radiotherapy,[11,12] chemotherapy[13,14] and immunotherapy,[15,16] but surgical resection can damage the function of the limb and most osteosarcoma is insensitive to radiotherapy, and there are many defects in chemotherapy. Currently, there are no specific drugs for treating osteosarcoma and traditional drugs usually causes severe toxicity and side effects, even multiple resistance. In addition, due to poor permeability of bone tissue, drug accumulating in bone tumors by traditional administration methods is far from satisfactory. Based on these observations, it is urgent to explore and discover effective treatment methods for such a common and serious disease.

Phototherapy, including photodynamic therapy and photothermal therapy, is a minimally invasive technique for tumor treatment.[17–19] Compared with traditional treatment methods, phototherapy has the following advantages:[20–23] (1) universal applicability: it has a therapeutic effect on a variety of tumors,

This journal is © The Royal Society of Chemistry and the Chinese Chemical Society 2019

Mater. Chem. Front., 2019, **3**, 1523–1531 | 1523

and after long-term follow-up and evaluation, it will not produce drug resistance; (2) targeting: it only acts on a specific tumor site, and the laser is only irradiated on the tumor tissue containing the photosensitizer, and does not cause damage to normal tissues; (3) minimally invasive: it only produces a killing effect on local tumors, and does not cause much damage to surrounding normal tissues and the whole body. By injecting a photosensitizer, a specific wavelength of visible light is used to locally irradiate the tumor area. Photochemical and photo-biological reactions produce high levels of reactive oxygen species (ROS),[24,25] which will induce apoptosis and necrosis at the site of the lesion.[26,27] While photothermal therapy is a therapeutic strategy in which photon energy is converted into heat to burn tumor cells to death, it also causes vascular damage, and microcirculatory disorders, and affects tumor blood supply.[28–30] From the view of synergistic therapy, combining PDT with photo-thermal therapy (PTT)[31–33] is a wise strategy for treatment of cancer. Nanomaterial-based PDT/PTT therapy is considered to be a promising treatment for bone tumors because of its specific killing and controllability in time and space.

Currently, the research progress of phototherapy in the treatment of osteosarcoma is relatively limited. The commonly used photosensitizers are also limited to acridine orange,[34,35] 5-aminolevulinic acid,[36,37] *meso*tetrahydroxyphenylchlorin (mTHPC),[38] hiporfin,[39] methylene blue[40] and so on. But these photosensitizers have many drawbacks, such as poor biosecurity, obvious side effects, low efficiency and poor penetration. Therefore, there is an urgent need to develop new photosensitizers that can inhibit the proliferation of osteosarcoma. BODIPY (boron-dipyrromethene)[41–46] derivatives are potential candidates for imaging guided phototherapy. In this study, we have designed and synthesized a new compound 10-(5-bromo-thiophen-2-yl)-3,7-bis((E)-4-(diphenylamino)styryl)-5,5-difluoro-1,9-dimethyl-5H-dipyrrolo[1,2-c:2′,1′-f][1,3,2]diazaborinin-4-ium-5-uide (BDPTPA), which has both photothermal and photodynamic effects. The singlet oxygen yield and photothermal conversion efficiency of BDPTPA were as high as 35.2% and 52.6%, respectively. By nanoprecipitation, soluble and stable BDPTPA NPs can be obtained and it has a wide absorption range which extends to the near-infrared region (600–1100 nm), showing a better ability to penetrate biological tissues. At the same time, the NPs can acquire passive targeting ability, which makes it easier for them to accumulate in the tumor tissue due the enhanced permeability and retention effect (EPR), and the *in vivo* fluorescence imaging illustrates this point. *In vitro* cell experiments proved that BDPTPA NPs have an excellent photo toxicity which can induce apoptosis of osteosarcoma cells, while good biological safety and little adverse effect on the viability of normal cells. Furthermore, *in vivo* experiments indicate that BDPTPA NPs also inhibit tumor growth in nude mice even without any side effects. Moreover, the pharmaco-kinetic studies reveal the process of absorption and distribu-tion of drugs in rats, and the terminal elimination half-lifes ($T_{1/2}$) of BDPTPA and BDPTPA NPs were 1.727 ± 0.415 and 5.639 ± 0.37 h, respectively, which also prove that BDPTPA NPs could be more suitable for treatment. Our results indicate that
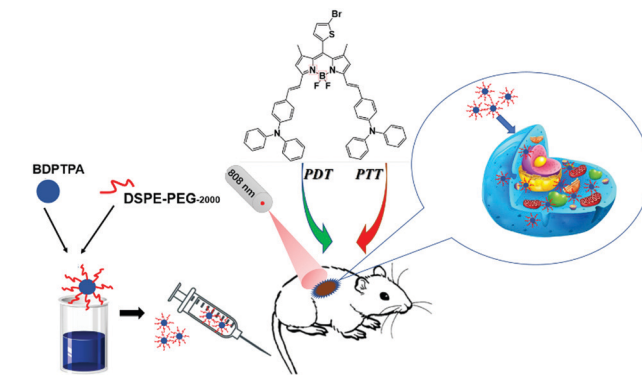
Scheme 1   Illustration of BDPTPA NPs for PDT/PTT synergistic therapy.

BDPTPA NPs are potential candidate for imaging guided photo-therapy in the clinic (Scheme 1).

Experimental

Materials and reagents

All the chemicals were purchased from Sigma-Aldrich. The ^{1}H NMR and ^{13}C NMR spectra were recorded in CDCl$_3$ solution on a Bruker DRX NMR spectrometer (500 MHz) with solvent residual as the internal standard. The UV-vis spectra were measured on a spectrophotometer (UV-3600, Shimadzu, Japan). The fluorescence spectra were recorded on a spectrometer (F-4600, HITACHI, Japan). The size of the nanoparticles was recorded by a particle size analyzer (90 Plus, Brookhaven Instruments, USA). The morphology of the nanoparticles was determined on a transmission electron microscope (JEM-2100, JEOL). The bio-images of the tumor, heart, liver, spleen, lung and kidneys were recorded on an imaging system (IVIS Lumina K, PerkinElmer).

Synthesis of BDPTPA

A mixture of 10-(5-bromothiophen-2-yl)-5,5-difluoro-1,3,7,9-tetra-methyl-5H-dipyrrolo[1,2-c:2′,1′-f][1,3,2]diazaborinin-4-ium-5-uide (0.409 g, 0.001 mol) and 4-(diphenylamino)benzaldehyde (0.820 g, 0.003 mol) was dissolved in DMF, which was heated at 120 °C using acetic acid (0.4 mL) and piperidine (0.4 mL) as a catalyst. Then the mixture was poured into brine, extracted with CH$_2$Cl$_2$ three times (10 mL), then washed with brine and dried with anhydrous sodium sulfate. The solvent was removed by rotary evaporation, and the crude product was purified by column chromatography (silica gel, DCM : PE = 1 : 2, v/v).

Preparation of nanoparticles of BDPTPA

The nanoparticles of the compound were prepared by nano-precipitation. In brief, a mixture of BDPTPA (10 mg) and DSPE-PEG$_{2000}$ (2 mg) was dissolved in tetrahydrofuran (1 mL). Then 200 µL of the solution was added into 10 mL of water under ultrasound at room temperature. The mixture was stirred for another 20 min to remove the tetrahydrofuran by nitrogen blowing. BDPTPA NPs in the solution were obtained by centrifugation.

1524 | *Mater. Chem. Front.,* 2019, **3**, 1523–1531

This journal is © The Royal Society of Chemistry and the Chinese Chemical Society 2019

Singlet oxygen detection in DCM and water

The singlet oxygen generation of BDPTPA was detected with 1,3-diphenylisobenzofuran (DPBF) which was used as a singlet oxygen detector. Briefly, 20 mM DPBF was added to the BDPTPA solution in a dark room. Then the mixture was irradiated using laser irradiation (808 nm, 1.0 W cm^{-2}). Methylene blue is used as a standard substance to calculate the singlet oxygen quantum yield of BDPTPA. SOSG (singlet oxygen sensor green) was used to detect the singlet oxygen generation of BDPTPA NPs. The fluorescence intensity of SOSG was recorded after irradiation at 492 nm.

Cell culture

The human osteosarcoma cell lines used in this study were obtained from Cell Bank of Shanghai Institute of Biochemistry and Cell Biology, Chinese Academy of Sciences. The MG-63 and HOS cells were cultured in Minimum essential medium (Gibco; Thermo Fisher Scientific) with 10% fetal bovine serum (FBS; Gibco; Thermo Fisher Scientific), and the U2OS and Saos-2 cells were cultured in McCoy's 5A (Modified) Medium (Thermo Fisher Scientific, Waltham, MA, USA) with 15% fetal FBS. The 143B and L02 cells were cultured in RPMI-1640 (Gibco; Thermo Fisher Scientific) with 10% fetal bovine serum, and the HEK-293, HUVEC and BEAS-2B cells were cultured in Dulbecco's minimum essential medium (Gibco; Thermo Fisher Scientific) with 10% FBS, and all of the complete culture media contain 100 units per mL penicillin and 100 μg per mL streptomycin. All the cells were cultured at 37 °C in a humidified incubator with 5% CO_2.

MTT assay

Cell viability of the nanoparticles was determined using a 3-(4,5-dimethylthiazol-2-yl)-2,5-diphenyltetrazolium bromide (MTT) colorimetric assay. Cells were seeded into 96-well plates with 1×10^4 per well in 100 μL culture medium. The cells were incubated for 24 h and then exposed to drug at various concentrations, and the control cells were treated with 0.5% DMSO. Then the 96-well plate was irradiated with a laser (808 nm, 0.5 W cm^{-2}) for 8 minutes. After that, the cells were still incubated for another 12 h. Subsequently, 10 μL MTT solution (5 mg mL^{-1} in PBS) was added and incubated for 4 h, Then the supernatants were removed and 100 μL DMSO was added to dissolve the formazan crystals. The absorbance was recorded at 492 nm by a Thermo Multiskan Mk3 Microplate Reader at ambient temperature. The cell viability was calculated by the following equation: cell viability (%) = ($A_{treatment}/A_{control}$) × 100% (mean absorbance in each group incubated with different concentrations of NPs/mean absorbance in the control group). The half-maximal inhibitory concentration (IC$_{50}$) was determined using GraphPad Prism 6 software (GraphPad Software, Inc., La Jolla, CA, USA).

Cellular uptake study

143B cells were incubated with BDPTPA NPs (1 μg mL^{-1}, 2 mL) in a confocal dish for 24 h in a 5% CO_2 incubator. Then the medium was removed and the cells were washed with PBS, followed by the addition of 1 mL 70% ethyl alcohol for 15 min at 4 °C. Then ethyl alcohol was discarded and the cells were washed with PBS three times. The fluorescence images are observed with an Olympus IX 70 inverted microscope excited with a 633 nm laser and collected from 650 to 750 nm.

Fluorescence imaging of cellular ROS

143B cells were seeded into a confocal dish and incubated with culture media at 37 °C for 24 hours in a 5% CO_2 incubator, followed by incubation with the media containing BDPTPA NPs (5 μg mL^{-1}, 1 mL) for an additional 24 h. Then, the cells were incubated with 2,7-dichlorodihydrofluorescein diacetate (DCFH-DA, 1 μg mL^{-1}, 2 mL) for 20 min. Then the cells were washed with PBS three times and irradiated with a laser (808 nm, 0.5 W cm^{-2}) for 10 min. The fluorescence images are observed by an Olympus IX 70 inverted microscope excited at 488 nm and collected from 500 to 600 nm for DCF detection.

Cell wound healing assay

143B cells were seeded into a 6-well culture plate with Culture-Inserts (IBIDI, German) in each well and incubated with culture media at 37 °C for 24 hours in a 5% CO_2 incubator. All cells were set up into three groups including control, illumination and without illumination groups. And then, cells in the illumination group were treated with the BDPTPA NPs (1 μg mL^{-1}) and irradiated with a laser for 5 min (808 nm, 0.5 cm^{-2}); without illumination group cells were only treated with BDPTAPA NPs at the same concentration while control group cells were incubated with fresh media. 12 h later, a cell-free gap of 500 μm was created after removing the Culture-Inserts, and cells in the three groups were allowed to migrate into the wound area. Images were captured using a Nikon Inverted Microscope (Nikon TS100, Nikon, Tokyo, Japan).

Transwell invasion assay

Cell invasion assays were evaluated in Transwell 24-well Boyden chambers (8.0 μm pore; BD Biosciences) precoated with 20 μg Matrigel (BD Bioscience) in a complete medium, and the group setting was the same as in the cell wound healing assay. Approximately 2×10^4 cells per mL 143B cells were plated in the top chamber with serum-free medium containing BDPTPA NPs, while the culture medium with 10% FBS was added to the bottom chamber; after that the cells were irradiated with a laser for 5 min (808 nm, 0.5 W cm^{-2}) and incubated at 37 °C for 24 hours. After treatment, the invaded cells were fixed and stained, photographed and counted under a microscope (Nikon TS100, Nikon, Tokyo, Japan).

Antitumor effects in nude mice of xenograft tumor models

28–35 day old male BALB/c nude mice, weighing 20 ± 2 g, were obtained from the Comparative Medicine Centre of Yangzhou University. The animal study was carried out according to the National Institutes of Health regulations and approved by the Institutional Animal Care and Use Committee. The 143B cells were injected subcutaneously into the nude mice at a density of

5×10^6 cells per 100 μL serum free medium, and the tumor size was measured every two days. When the tumor volume reaches about 100 mm^3, the mice were randomly divided into three groups: (i) a control group with tail vein injection of saline solution; (ii) an illumination group with injection of BDPTPA NPs and under irradiation; (iii) a without illumination group with intravenous injection of BDPTPA NPs without irradiation. 10 μg (100 μg mL^{-1}, 100 μL) BDPTPA NPs were injected into such mice *via* the tail vein for the illumination and without illumination groups, respectively, while the control group was injected with PBS. After administration, the tumors of the control and illumination groups were irradiated by an 808 nm laser for 8 minutes while the mice in the no illumination group were not irradiated. Tumor volume (V) was measured daily to observe dynamic changes in tumor growth and calculated according to the formula: V (mm^3) = length × width^2 × 0.5. The treatment process was conducted for twenty days, and the tumor volume and body weight of the mice were recorded every two days. At the end of treatment, all the nude mice were sacrificed and the tumor tissues were removed and measured for histopathological assay. Some major organs (heart, liver, spleen, lung, and kidney) were removed for histopathological examination to evaluate drug toxicity.

In vivo imaging

100 μL BDPTPA NPs (100 μg mL^{-1}) solution in PBS was administered into nude mice through tail intravenous injection. At different time points after tail intravenous injection, *in vivo* fluorescence images were recorded using an Endra Nexus128 small animal imaging system. The temperature was also monitored using an FLIR thermal camera under irradiation of an 808 nm laser for 10 min, 6 h post-injection. The mice injected with saline were evaluated as a control.

Pharmacokinetic study

Twelve Sprague-Dawley rats (six males and six females, 220 ± 10.0 g) were obtained from the Animal Center of Nanjing Medical University (NJMU, Nanjing, China). The animals were housed under standard conditions and had free access to food and water. This animal study was reviewed and approved by the Animal Ethical Committee of Nanjing Tech University.

Twelve rats were given BDPTPA NPs and BDPTPA molecular solution dissolved in saline containing 10% DMSO at the same dose of 5 mg kg^{-1} *via* tail vein injection. Blood samples (0.2 mL) were collected in heparinized Eppendorf tubes from the ophthalmic venous plexus at 0 (pre-dose), 0.083, 0.25, 0.5, 1, 2, 4, 6, 8, 12 and 24 h after intravenous (i.v.) administration. Plasma was separated by centrifuging the blood at 3000 × g for 10 min at 4 °C and stored at −70 °C until analysis.

The standard stock solutions of BDPTPA and BDPTPA NPs were accurately prepared in DMSO and PBS solutions. A series of standard working solutions for BDPTPA was prepared by diluting the stock solution with DMSO to concentrations in the range of 12.5–500 μg mL^{-1}, while the working solutions for BDPTPA NPs were diluted with PBS in the same range. Subsequently, the calibration standards were prepared by spiking

20 μL BDPTPA or BDPTPA NPs into 180 μL blank rat plasma at concentrations of 1.25, 2.5, 5, 10, 20, and 50 μg mL^{-1}. The standard curve samples and the rat plasma samples were transferred to a micro cuvette and analyzed by an ultraviolet spectrophotometer.

The pharmacokinetic parameters were calculated by a non-compartmental method using DAS 3.0 software (Mathematical Pharmacology Professional Committee of China, Shanghai, China). The area under the curve (AUC) from zero to the last measurable plasma concentration point (AUC$_{0-t}$), AUC from zero to infinity (AUC$_{0-\infty}$), the elimination rate constant (K), the terminal elimination half-life ($T_{1/2}$), mean residence time (MRT), and systemic clearance (CL) were calculated by the software.

Results and discussion

Synthesis and characterization of BDPTPA and NPs

The synthetic procedure of BDPTPA is proposed in the ESI† (Fig. S1). All the intermediates and products have been fully structurally characterized by ^{1}H NMR (Fig. S2, ESI†), ^{13}C NMR (Fig. S3, ESI†) and mass spectrometry (Fig. S4, ESI†). For ^{1}H NMR (CDCl$_3$, 400 MHz): δ (ppm) 7.61–7.54 (2H, d), 7.48–7.43 (4H, d), 7.31–7.28 (2H, d), 7.25–7.22 (3H, d), 7.21–7.15 (2H, d), 7.14–7.09 (9H, d), 7.09–7.04 (6H, m), 7.04–6.98 (5H, d), 6.79–6.76 (1H, d), 6.63 (2H, s), 1.74 (6H, s). ^{13}C NMR (75 MHz, CDCl$_3$): δ 153.15, 148.67, 147.05, 141.52, 136.18, 130.24, 129.39, 128.67, 125.18, 123.49, 122.34, 118.06, 117.23, 31.55, 30.13, 29.68, 14.23. MS (ESI): calcd m/z = 918.2; found m/z = 921.7.

Since the compound can be hardly dissolved in water, the water-soluble BDPTPA NPs were prepared through a simple re-precipitation method. In general, 10 mg of BDPTPA was dissolved in THF, and 200 μL of such solution was injected into 10 mL distilled water with stirring. After being purged with nitrogen for 20 min to drive the THF off, the concentration of the obtained solution is 200 μg mL^{-1}.

As shown in Fig. 1a, BDPTPA NPs present a broad absorption range and the absorption peak was observed at 750 nm, while BDPTPA in DCM shows absorption with maximum intensity of 720 nm, which shows a red-shift of 30 nm caused by aggregation into nanoparticles, and BDPTPA show emission with maximum intensity at 780 nm (Fig. 1b), while a red shift of 40 nm was found for its nanoparticles. BDPTPA shows emissions with maximum intensity at 790 nm, while a red shift of 30 nm was found for its nanoparticles. Then, the morphology and diameter of the nanoparticles was characterized by a transmission electron microscope (TEM) and dynamic light scattering (DLS). As shown in Fig. 1e, the morphology of the nanoparticles showed well defined spherical nanostructures, and the average diameter distribution was from approximately 40 to 160 nm. In order to achieve deep tissue penetration in the NIR window, the BDPTPA NPs were used in the subsequent experiments.

A high singlet oxygen quantum yield (QY) is fundamental to PDT efficacy. 1,3-Diphenylisobenzofuran (DPBF) was used as a

1526 | *Mater. Chem. Front.*, 2019, **3**, 1523–1531

This journal is © The Royal Society of Chemistry and the Chinese Chemical Society 2019
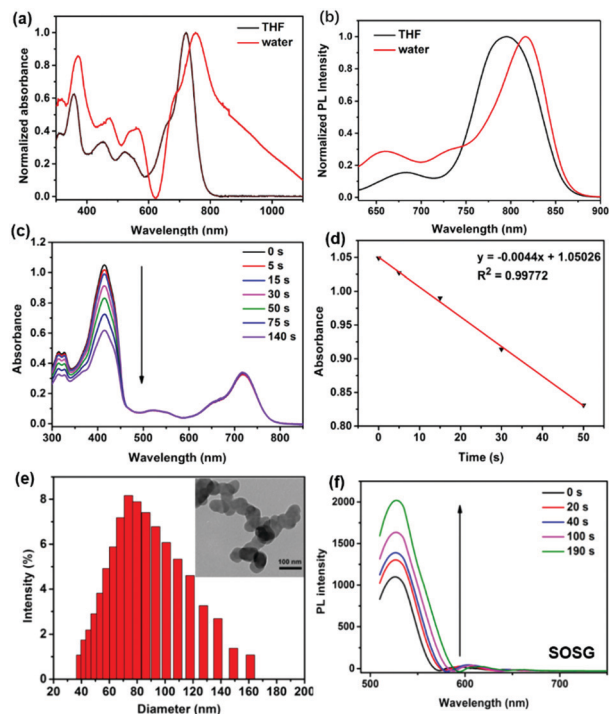
Fig. 1 Normalized (a) absorption and (b) emission spectra of BDPTPA in THF and NPs in water. (c) The degradation of DPBF in the presence of BDPTPA in DCM and 660 nm laser irradiation. (d) Linear fitting of the absorption and the irradiation time. (e) The DLS size distribution of the BDPTPA NPs. Inset: A TEM image of BDPTPA NPs. (f) Fluorescence enhancement of SOSG with laser irradiation (808 nm, 0.5 W cm^{-2}).
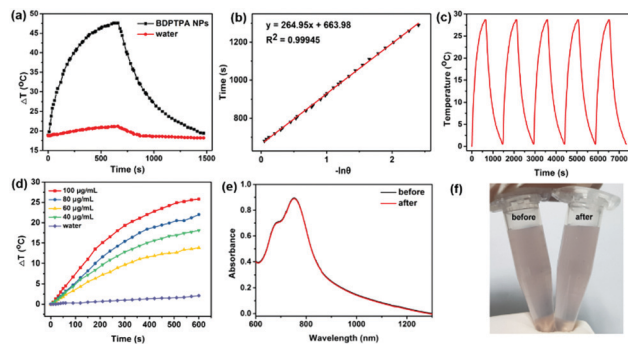

Fig. 2 (a) Temperature increase of water and BDPTPA NPs with laser irradiation (water was irradiated as a control). (b) Linear fitting of $-\ln\theta$ and time in the cooling curve. (c) The heating curve of the BDPTPA NPs at a concentration of 100 mg mL^{-1} during five cycles. (d) The heating curves of the BDPTPA NPs with different concentrations. (e and f) The absorbance spectra and color of the BDPTPA NPs before/after laser irradiation.

probe to measure the singlet oxygen QY of BDPTPA in DCM, the absorption of DPBF was recorded under irradiation for different times. With methylene blue (MB) as the standard substance ($\Phi_\Delta = 0.57$ in DCM) (Fig. S5, ESI†), the singlet oxygen QYs were calculated according to the literature[47] and demonstrated an outstanding singlet oxygen generation efficiency. As shown in Fig. 1c and d, in the presence of BDPTPA, the DPBF degrades at a high speed, compared with that of MB. The calculated $^1O_2$ QY of BDPTPA is 35.2%. At the same time, SOSG (singlet oxygen sensor green) was used to evaluate the singlet oxygen of BDPTPA NPs in PBS solution. Fig. 1f shows that the fluorescence intensity of SOSG has been greatly enhanced with laser irradiation, suggesting the high singlet generation ability of BDPTPA NPs.

Furthermore, the near-infrared absorption indicates that the BDPTPA NPs also possess high photothermal conversion ability. The photothermal conversion ability of BDPTPA NPs was calculated by recording the temperature elevation with irradiation in the presence of BDPTPA NPs and a cooling process without irradiation. As illustrated in Fig. 2a, a temperature increase of 28.7 °C could be observed with low power laser irradiation (808 nm, 0.5 W cm^{-2}) while a negligible one was observed for water, of only 2.8 °C, indicating the excellent photothermal conversion ability of such NPs. According to the equation described in the previous report,[48] the photothermal conversion efficiency (η) was calculated to be 52.6%.

Fig. 2e shows the light-to-heat cycling stability of the BDPTPA NPs. There is no decrease in the temperature elevation after five cycles, and the color of the BDPTPA NPs has no changes before and after irradiation for five cycles (Fig. 2c and f); all these results reveal that the BDPTPA NPs have good photothermal stability. In addition, BDPTPA NPs with different concentrations (20, 40, 60, 80 μg mL^{-1}) were used to examine the photothermal conversion ability under the same conditions; as shown in Fig. 2d, the temperature increase of the BDPTPA NPs is obviously concentration-dependent under laser irradiation.

BDPTPA induced apoptosis in human osteosarcoma cells

To validate the synergistic phototherapeutic effects of BDPTPA NPs, we evaluated the inhibitory effect of BDPTPA NPs on the cell viability of human osteosarcoma cells including HOS, U-2OS, MG-63 and 143B cells at different concentrations. After treatment of BDPTPA NPs for 24 h, MTT assay shows that the IC$_{50}$ (the concentration of drug inhibiting 50% of cells) values of HOS, U-2OS, MG-63 and 143B cells were 4.38, 5.729, 5.862 and 3.996 μg mL^{-1} respectively (Fig. 3a–d). In addition, the group incubated with the nanoparticles without irradiation have low dark toxicity. At the same time, the normal human cells including HEK-293 (Human Embryonic Kidney 293 cells), HUVEC (Human Umbilical Vein Endothelial Cells), L02 (Human L02 hepatocytes) and BEAS-2B (Human Bronchial Epithelial Cells) were used to evaluate the dark toxicity, and the results also show that the BDPTPA NPs have low dark toxicity to normal cells (Fig. S6, ESI†).

And then Annexin V-FITC/PI double staining assay was used to confirm the pro-apoptotic effect of BDPTPA NPs. Compared with a control group, the results demonstrated that the apoptotic rates of 143B cells in the illumination group were significantly increased after treatment with BDPTPA NPs (5 μg mL^{-1}), while the apoptotic rate of the without illumination group was similar to that of the control group (Fig. 3e), which demonstrates that BDPTPA NPs can induce typical apoptosis in human osteosarcoma cells under irradiation.
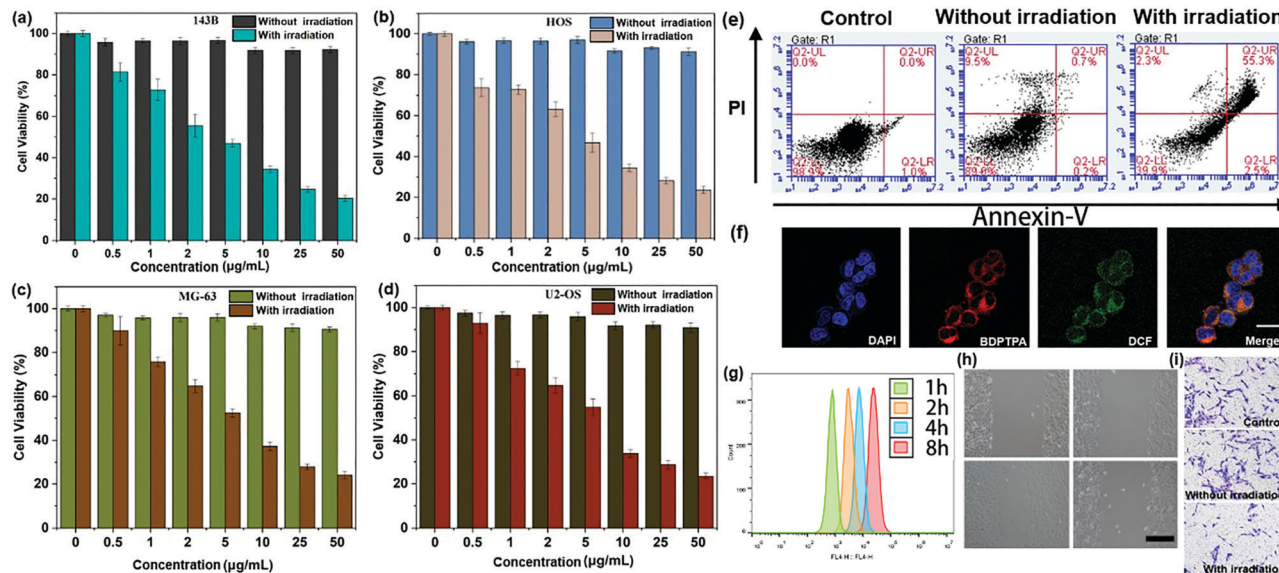
This journal is © The Royal Society of Chemistry and the Chinese Chemical Society 2019

Mater. Chem. Front., 2019, 3, 1523–1531 | 1527

Fig. 3 MTT assay of BDPTPA NPs with different concentrations on four osteosarcoma cells. (a) 143B; (b) HOS; (c) MG-63; (d) U2-OS. (e) The apoptotic rates of 143B cells induced by BDPTPA NPs were detected by Annexin V/PI double-staining assay. (f) Cellular uptake of BDPTPA NPs and ROS generation with DCF-DA as a probe. Scale bar: 10 μm. (g) Cellular uptake by flow cytometry fluorescence enhancement at different times. (h) 143B cell migration in the scratch-wound healing assay. Scale bar: 100 μm. (i) The transwell migration assay of 143B cells.

In vitro cell migration and invasion of osteosarcoma cells

The property of inhibiting cell migration is important for a photosensitizer, because osteosarcoma tumors are highly metastatic *in vivo*. Firstly, the "wound-healing" assays were used to investigate the effect of BDPTPA NPs on cell migration. As shown in Fig. 3g, it is obvious to observe that 143B cells in the control group moved and filled in the open gap at 24 h after wounding, while BDPTPA NPs treatment with illumination dramatically suppressed wound closure even at a low concentration (1 μg mL^{-1}). These results show that BDPTPA NPs can effectively inhibit the migration of osteosarcoma cells, which might have the potential of inhibiting tumor metastasis *in vivo*.

And then Transwell experiments were used to verify the ability of inhibiting cell invasion under the treatment of BDPTPA NPs (Fig. 3h). These results showed that BDPTPA NPs could inhibit the migration and invasion of osteosarcoma cells *in vitro* without cytotoxicity, demonstrating that BDPTPA NPs could be a potential and multiple functional agent for treating human osteosarcoma tumors.

Cellular uptake and ROS generation *in vitro*

A confocal living cell imaging system was used to investigate the cellular uptake behaviors of BDPTPA NPs. The cellular uptake of BDPTPA NPs is shown in Fig. 3f. A high intracellular fluorescence intensity in the cytoplasmic matrix can be observed, indicating that the BDPTPA NPs can be used for cell imaging *in vitro*. Further flow cytometry confirms the uptake of BDPTPA NPs in 143B cells due to the time dependent fluorescence enhancement.

2′,7′-Dichlorofluorescein diacetate (DCF-DA) was used to investigate the ROS generation of BDPTPA NPs in cells. As shown in Fig. 3f, strong green fluorescence can be observed,

indicating that BDPTPA NPs are able to generate strong singlet oxygen under irradiation *in vitro*.

In vivo fluorescence imaging guided phototherapy

Fig. 4a shows the fluorescence images of tumor tissues at different times after the tail vein injection of BDPTPA NPs (100 μg mL^{-1}, 100 μL). The fluorescence signals of the tumors increased rapidly and maintained a high level from 1 to 24 h after injection, suggesting that BDPTPA NPs can be effectively accumulated at tumor sites because of the enhanced permeability and retention (EPR) effect. The results show that after 6 h injection, the fluorescence intensity reached a maximum level, suggesting that 6 hour may be suitable for PDT after administration. Furthermore, after 24 h injection, the fluorescence signal of the tumor was still at a high level, indicating that BDPTPA NPs can be used as a long-term fluorescence imaging agent. Finally, the mice were sacrificed and the biodistribution shows that BDPTPA NPs mainly stay in the tumor, liver and kidneys (Fig. 4a and b).

Pharmacokinetic studies in rats

The sensitive and specific ultraviolet spectrophotometer was applied in the pharmacokinetic study of BDPTPA and BDPTPA NPs after intravenous administration. The mean plasma concentration–time profiles of BDPTPA and BDPTPA NPs are shown in Fig. 5a. The major pharmacokinetic parameters were calculated by a non-compartmental model and are presented in Table 1. The values of the AUC$_{(0-t)}$/AUC$_{(0-\infty)}$ were more than 80% suggesting that the blood collection time point was suitable for the pharmacokinetic studies. The data showed that the BDPTPA eliminated much more quickly than BDPTPA NPs, the terminal elimination half-life ($T_{1/2}$) was 1.727 ± 0.415 and

1528 | *Mater. Chem. Front.*, 2019, **3**, 1523–1531

This journal is © The Royal Society of Chemistry and the Chinese Chemical Society 2019
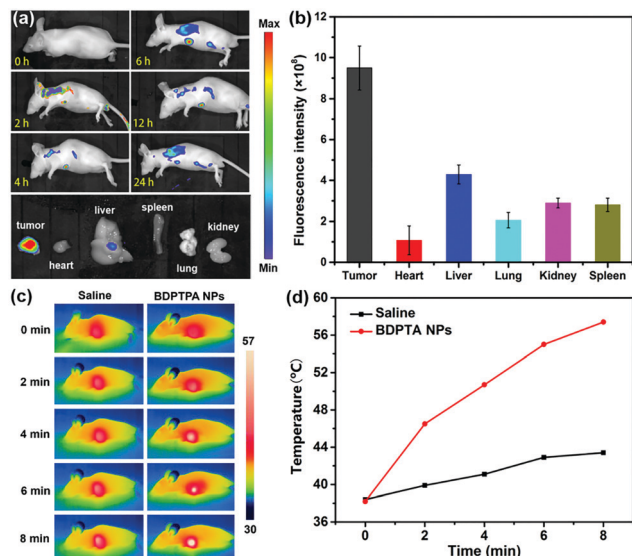
Fig. 4 (a) *In vivo* time dependent fluorescence imaging and bio-distribution of BDPTPA NPs in the tumor, heart, liver, spleen, lungs and kidneys after injection for 24 h. (b) Fluorescence intensity of the tumor, heart, liver, lungs, spleen, and kidneys. (c) *In vivo* photothermal imaging of the nude mice after injection with saline or BDPTPA NPs under laser irradiation. (d) Temperature increase of the group injected with saline or BDPTPA NPs under laser irradiation.
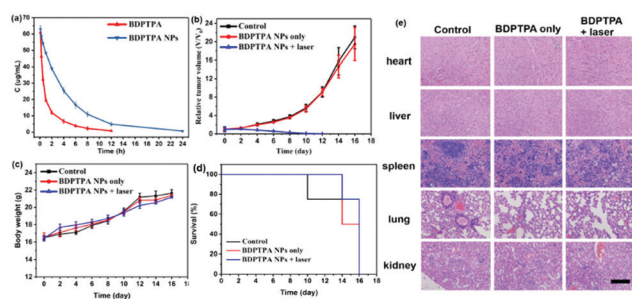

Fig. 5 (a) Mean plasma concentration–time curves of BDPTPA and BDPTPA NPs after a single intravenous administration at a dose of 5 mg kg^{-1} in rats. (b) Relative tumor volume. (c) Body weight change of three groups. (d) Survival of the mice during treatment. (e) H&E stained images of the heart, liver, spleen, lungs, and kidneys of three groups, respectively. Scale bar: 100 μm.

5.639 ± 0.37 h for BDPTPA and BDPTPA NPs, respectively. The CLz of BDPTPA was 0.053 ± 0.003 L h^{-1} kg^{-1} while the value of BDPTPA NPs was 0.016 ± 0.001 L h^{-1} kg^{-1}, which also indicated that the BDPTPA NPs eliminated slower than BDPTPA in rats, and all the results show that the BDPTPA NPs could extend the residence time in rats and promote its treatment effects.

In vivo photothermal imaging and phototherapy

To further investigate the PDT and PTT synergistic therapeutic efficacy of BDPTPA NPs *in vivo*, 12 nude mice bearing osteosarcoma tumors were used in this study. As shown in Fig. 4c, under irradiation, the tumor surface temperature increased

Table 1 Non-compartmental pharmacokinetic parameters of BDPTPA and BDPTPA NPs in rat plasma after a single intravenous administration at a dose of 5 mg kg^{-1} (n = 6)

Parameter	Unit	BDPTPA in DMSO (10%)	BDPTPA NPs
$T_{1/2}$	H	1.727 ± 0.415	5.639 ± 0.37
$AUC_{(0-t)}$	mg L^{-1} h	93.744 ± 5.297	298.588 ± 12.477
$AUC_{(0-\infty)}$	mg L^{-1} h	94.586 ± 5.081	307.545 ± 14.671
$MRT_{(0-t)}$	H	2.274 ± 0.415	4.717 ± 0.161
CL_z	L h^{-1} kg^{-1}	0.053 ± 0.003	0.016 ± 0.001
V_z	L kg^{-1}	0.132 ± 0.035	0.132 ± 0.003

$T_{1/2}$: terminal elimination half-life; AUC_{0-t}: the area under the curve from zero to the last measurable plasma concentration point; $AUC_{0-\infty}$: the area under the curve from zero to infinity; $MRT_{(0-t)}$: mean residence time; CL_z: systematic clearance; V_z: apparent volume of distribution.

rapidly with 8 min compared with the control group. Fig. 5b shows that the tumor volume of the control and the without illumination group increase at a high speed. While after the irradiation treatment, the tumor volume was not significantly increased in the illumination group; after treatment six times, the tumor of the illumination group even disappears at the end of the therapy process, and all the mice were still raised for another 6 days, and no obvious tumors were observed. All of these results indicate that BDPTPA NPs have high phototoxicity and efficiency for tumor treatment. The tumor volume and body weight were recorded every two days.

Though BDPTPA NPs inhibited the growth of tumors *in vivo*, their potential toxicity must be assessed comprehensively. During the treatment process, no significant difference between the body weight of the mice in the three groups was observed (Fig. 5c), which indicates the low dark toxicity of BDPTPA NPs. The cured mice in the illumination group are shown in Fig. S7 (ESI†).

After the treatment, all the mice were sacrificed and the tumors were collected as well as the normal organs, including heart, liver, spleen, lungs, and kidneys. The trend of the tumor is shown in Fig. 5d. According to the hematoxylin and eosin (H&E)-stained images, we also found no obvious change in normal organs between control and BDPTPA NPs treated groups (Fig. 5e). The results indicated that BDPTPA NPs exerted anti-tumor activity without any toxicity *in vivo*. The blood index, liver function and renal function of the mice injected with BDPTPA NPs are the same as those in the control group (Table S, ESI†). The results indicated that BDPTPA NPs can inhibit tumor growth effectively without damaging the normal organs, suggesting their good bio-compatibility.[49–54]

Conclusions

In conclusion, BDPTPA with both photodynamic and photothermal effects was designed and synthesized. The results show that BDPTPA presents high singlet oxygen generation efficiency (35.2%) as well as high photothermal conversion efficiency (52.6%). *In vitro* experiments suggest that BDPTPA NPs could induce significant apoptosis of osteosarcoma cells with irradiation, while they have no effect on the viability of normal cells

This journal is © The Royal Society of Chemistry and the Chinese Chemical Society 2019

Mater. Chem. Front., 2019, **3**, 1523–1531 | **1529**

under dark conditions. In addition, such NPs can inhibit the migration of osteosarcoma cells, confirmed by the cell migration and transwell experiments. In *in vivo* experiments, the BDPTPA NPs could accumulated in tumor tissues by the EPR effect and inhibit tumor growth without any side effects in nude mice. Moreover, the BDPTPA NPs have a good pharmacokinetic characteristic in contrast to BDPTPA. Both *in vitro* and *in vivo* experiments indicate that the BDPTPA NPs have an excellent photo toxicity, low dark toxicity and good biocompatibility. Therefore, BDPTPA is a promising multi-functional agent for the treatment of osteosarcoma.

Conflicts of interest

The authors have no conflict of interest to declare.

Acknowledgements

Notes and references

1 L. Mirabello, R. J. Troisi and S. A. Savage, *Int. J. Cancer*, 2009, **125**, 229–234.

2 S. S. Bielack, S. Hecker-Nolting, C. Blattmann and L. Kager, *F1000Research*, 2016, **5**, 2767.

3 S. S. Bielack, B. Kempf-Bielack, G. Delling, G. U. Exner, S. Flege, K. Helmke, R. Kotz, M. Salzer-Kuntschik, M. Werner, W. Winkelmann, A. Zoubek, H. Jurgens and K. Winkler, *J. Clin. Oncol.*, 2002, **20**, 776–790.

4 S. Bielack, B. Kempf-Bielack, T. Von Kalle, R. Schwarz, T. Wirth, L. Kager and J. Whelan, *Minerva Pediatr.*, 2013, **65**, 125–148.

5 S. Ferrari and M. Serra, *Expert Opin. Pharmacother.*, 2015, **16**, 2727–2736.

6 L. Kager, A. Zoubek, U. Potschger, U. Kastner, S. Flege, B. Kempf-Bielack, D. Branscheid, R. Kotz, M. Salzer-Kuntschik, W. Winkelmann, G. Jundt, H. Kabisch, P. Reichardt, H. Jurgens, H. Gadner, S. S. Bielack and G. Cooperative German-Austrian-Swiss Osteosarcoma Study, *J. Clin. Oncol.*, 2003, **21**, 2011–2018.

7 M. E. Anderson, *Orthopedic Clinics of North America*, 2016, vol. 47, pp. 283–292.

8 A. Longhi, C. Errani, M. De Paolis, M. Mercuri and G. Bacci, *Cancer Treat. Rev.*, 2006, **32**, 423–436.

9 H. Wafa and R. J. Grimer, *Expert Rev. Anticancer Ther.*, 2006, **6**, 239–248.

10 K. Ando, M. F. Heymann, V. Stresing, K. Mori, F. Redini and D. Heymann, *Cancers*, 2013, **5**, 591–616.

11 P. Agostinis, K. Berg, K. A. Cengel, T. H. Foster, A. W. Girotti, S. O. Gollnick, S. M. Hahn, M. R. Hamblin, A. Juzeniene, D. Kessel, M. Korbelik, J. Moan, P. Mroz, D. Nowis, J. Piette, B. C. Wilson and J. Golab, *Ca-Cancer J. Clin.*, 2011, **61**, 250–281.

12 A. Matsunobu, R. Imai, T. Kamada, T. Imaizumi, H. Tsuji, H. Tsujii, Y. Shioyama, H. Honda, S. Tatezaki and W. G. B. S. T. Sarco, *Cancer*, 2012, **118**, 4555–4563.

13 D. Carrle and S. S. Bielack, *Int. Orthop.*, 2006, **30**, 445–451.

14 G. Rosen, B. Caparros, A. G. Huvos, C. Kosloff, A. Nirenberg, A. Cacavio, R. C. Marcove, J. M. Lane, B. Mehta and C. Urban, *Cancer*, 1982, **49**, 1221–1230.

15 R. Luksch, D. Perotti, G. Cefalo, C. G. Passerini, M. Massimino, F. Spreafico, M. Casanova, A. Ferrari, M. Terenziani, D. Polastri, F. Gambirasio, M. Podda, F. Bozzi, F. Ravagnani, G. Parmiani and F. F. Bellani, *Tumori*, 2003, **89**, 263–268.

16 C. Liebau, C. Roesel, S. Schmidt, C. Karreman, J. B. Prisack, H. Bojar, H. Merk, N. Wolfram and A. W. Baltzer, *Anticancer Res.*, 2004, **24**, 2861–2867.

17 S. Yanase, J. Nomura, Y. Matsumura, Y. Watanabe and T. Tagawa, *Photomed. Laser Surg.*, 2009, **27**, 791–797.

18 A. Konski, *Cancer*, 2010, **116**, 3754–3755.

19 L. L. Sun, Y. J. Li, H. Y. Li, J. Zhang, B. H. Li and Z. M. Ye, *Clin. Ther.*, 2014, **36**, 567–578.

20 M. Ethirajan, Y. Chen, P. Joshi and R. K. Pandey, *Chem. Soc. Rev.*, 2011, **40**, 340–362.

21 L. Lin, L. Xiong, Y. Wen, S. Lei, X. Deng, Z. Liu, W. Chen and X. Miao, *J. Biomed. Nanotechnol.*, 2015, **11**, 531–554.

22 T. G. S. Denis and M. R. Hamblin, *Bioanalysis*, 2013, **5**, 1099–1114.

23 L. Cheng, C. Wang, L. Z. Feng, K. Yang and Z. Liu, *Chem. Rev.*, 2014, **114**, 10869–10939.

24 Z. Zhen, W. Tang, Y. J. Chuang, T. Todd, W. Zhang, X. Lin, G. Niu, G. Liu, L. Wang, Z. Pan, X. Chen and J. Xie, *ACS Nano*, 2014, **8**, 6004–6013.

25 C. S. Jin, J. F. Lovell, J. Chen and G. Zheng, *ACS Nano*, 2013, **7**, 2541–2550.

26 J. P. Wang, R. Yan, F. Guo, M. Yu, F. P. Tan and N. Li, *Nanotechnology*, 2016, **27**, 285102.

27 A. E. O'Connor, W. M. Gallagher and A. T. Byrne, *Photochem. Photobiol.*, 2009, **85**, 1053–1074.

28 F. van Leeuwen-vanZaane, H. S. de Bruijn, A. van der Ploeg-van den Heuvel, H. J. M. C. Sterenborg and D. J. Robinson, *Photodiagn. Photodyn. Ther.*, 2014, **11**, 71–81.

29 R. Weijer, M. Broekgaarden, M. Krekorian, L. K. Alles, A. C. van Wijk, C. Mackaaij, J. Verheij, A. C. van der Wal, T. M. van Gulik, G. Storm and M. Heger, *Oncotarget*, 2016, **7**, 3331–3346.

30 Z. P. Zhen, W. Tang, Y. J. Chuang, T. Todd, W. Z. Zhang, X. Lin, G. Niu, G. Liu, L. C. Wang, Z. W. Pan, X. Y. Chen and J. Xie, *ACS Nano*, 2014, **8**, 6004–6013.

31 D. de Melo-Diogo, C. Pais-Silva, D. R. Dias, A. F. Moreira and I. J. Correia, *Adv. Healthcare Mater.*, 2017, **6**, 1700073.

32 U. Lindner, N. Lawrentschuk, R. A. Weersink, S. R. Davidson, O. Raz, E. Hlasny, D. L. Langer, M. R. Gertner, T. Van der Kwast, M. A. Haider and J. Trachtenberg, *Eur. Urol.*, 2010, **57**, 1111–1114.

33 K. Ahrar, A. Gowda, S. Javadi, A. Borne, M. Fox, R. McNichols, J. U. Ahrar, C. Stephens and R. J. Stafford, *J. Vasc. Intervent. Radiol.*, 2010, **21**, 555–561.

34 C. Fotia, S. Avnet, K. Kusuzaki, L. Roncuzzi and N. Baldini, *Curr. Pharm. Des.*, 2015, **21**, 4088–4094.

35 H. Satonaka, K. Kusuzaki, K. Akeda, M. Tsujii, T. Iino, T. Uemura, T. Matsubara, T. Nakamura, K. Asanuma, A. Matsumine and A. Sudo, *Anticancer Res.*, 2011, **31**, 4163–4168.

36 S. Yanase, J. Nomura, Y. Matsumura, T. Nagata, T. Fujii and T. Tagawa, *Int. J. Oncol.*, 2006, **29**, 365–373.

37 I. Coupienne, G. Fettweis and J. Piette, *Lasers Surg. Med.*, 2011, **43**, 557–564.

38 D. Meier, C. Campanile, S. M. Botter, W. Born and B. Fuchs, *J. Visualized Exp.*, 2014, e51213, DOI: 10.3791/51213.

39 M. X. Sun, C. H. Zhou, H. Zeng, N. Puebla-Osorio, E. Damiani, J. Chen, H. S. Wang, G. D. Li, F. Yin, L. C. Shan, D. Q. Zuo, Y. X. Liao, Z. Y. Wang, L. P. Zheng, Y. Q. Hua and Z. D. Cai, *Photochem. Photobiol.*, 2015, **91**, 533–544.

40 T. Matsubara, K. Kusuzaki, A. Matsumine, H. Satonaka, K. Shintani, T. Nakamura and A. Uchida, *In Vivo*, 2008, **22**, 297–303.

41 H. J. Wories, J. H. Koek, G. Lodder, J. Lugtenburg, R. Fokkens, O. Driessen and G. R. Mohn, *Recl. Trav. Chim. Pays-Bas*, 1985, **104**, 288–291.

42 J. Chen, A. Burghart, A. Derecskei-Kovacs and K. Burgess, *J. Org. Chem.*, 2000, **65**, 2900–2906.

43 J. Chen, A. Burghart, C. W. Wan, L. Thia, C. Ortiz, J. Reibenspies and K. Burgess, *Tetrahedron Lett.*, 2000, **41**, 2303–2307.

44 K. Rurack, M. Kollmannsberger, U. Resch-Genger and J. Daub, *J. Am. Chem. Soc.*, 2000, **122**, 968–969.

45 X. Qi, E. J. Jun, L. Xu, S. J. Kim, J. S. J. Hong, Y. J. Yoon and J. Y. Yoon, *J. Org. Chem.*, 2006, **71**, 2881–2884.

46 M. Tasior, J. Murtagh, D. O. Frimannsson, S. O. McDonnell and D. F. O'Shea, *Org. Biomol. Chem.*, 2010, **8**, 522–525.

47 H. X. Shi, W. C. Sun, C. B. Liu, G. Y. Gu, B. Ma, W. L. Si, N. N. Fu, Q. Zhang, W. Huang and X. C. Dong, *J. Mater. Chem. B*, 2016, **4**, 113–120.

48 S. Ghosh, T. Avellini, A. Petrelli, I. Kriegel, R. Gaspari, G. Almeida, G. Bertoni, A. Cavalli, F. Scotognella, T. Pellegrino and L. Manna, *Chem. Mater.*, 2016, **28**, 4848–4858.

49 Z. Yang, Y. Dai, L. Shan, Z. Shen, Z. Wang, B. C. Yung, O. Jacobson, Y. Liu, W. Tang, S. Wang, L. Lin, G. Niu, P. Huang and X. Chen, *Nanoscale Horiz.*, 2019, **4**, 426–433.

50 Z. Yang, W. Fan, W. Tang, Z. Shen, Y. Dai, J. Song, Z. Wang, Y. Liu, L. Lin, L. Shan, Y. Liu, O. Jacobson, P. Rong, W. Wang and X. Chen, *Angew. Chem., Int. Ed.*, 2018, **130**, 14297–14301.

51 J. Yang, X. Q. Gu, W. T. Su, X. Y. Hao, Y. J. Shi, L. Y. Zhao, D. F. Zou, G. W. Yang, Q. Y. Li and J. H. Zou, *Mater. Chem. Front.*, 2018, **2**, 1842–1846.

52 Z. Yang, Y. Dai, C. Yin, Q. Fan, W. Zhang, J. Song, G. Yu, W. Tang, W. Fan, B. C. Yung, J. Li, X. Li, X. Li, Y. Tang, W. Huang, J. Song and X. Chen, *Adv. Mater.*, 2018, **30**, 1707509.

53 Z. Yang, R. Tian, J. Wu, Q. Fan, B. C. Yung, G. Niu, O. Jacobson, Z. Wang, G. Liu, G. Yu, W. Huang, J. Song and X. Chen, *ACS Nano*, 2017, **11**, 4247–4255.

54 Z. Yang, J. Song, Y. Dai, J. Chen, F. Wang, L. Lin, Y. Liu, F. Zhang, G. Yu, Z. Zhou, W. Fan, W. Huang, Q. Fan and X. Chen, *Theranostics*, 2017, **7**, 2177.

This journal is © The Royal Society of Chemistry and the Chinese Chemical Society 2019

Mater. Chem. Front., 2019, **3**, 1523–1531 | **1531**